Proceedings of the 23rd International Conference on Automation & Computing, University of Huddersfield, Huddersfield, UK, 7-8 September 2017

Planetary Gear Fault Diagnosis Based on Instantaneous Angular Speed Analysis

Qiang Zeng [a,b], Mones Zainab [a], Yimin Shao[b], Fengshou Gu[a], Andrew D. Ball [a]

[a] School of Computing and Engineering
University of Huddersfield
Huddersfield, UK

[b] State Key Laboratory of Mechanical Transmission
Chongqing University
Chongqing, P. R. China

***Abstract*— Planetary Gears (PG) are widely used in many important transmission systems such as helicopters and wind turbines due to its advantages of high power-weight ratio, self-centering and high transmission ratio. Vibration based condition monitoring of PG has received extensive researches for ensuring safe operations of these critical systems. However, due to the moving mesh gears and noise influences, the diagnostics of planet gear faults by conventional vibration measurements needs intensive signal processing but provides less satisfactory performance. This study investigates Instantaneous Angular Speed (IAS) based diagnostics which associates more directly with gear dynamics and is not influenced by the moving mesh gears. A pure torsional dynamic model of a PG is developed to gain the characteristics of IAS under different fault cases. Then experiments are performed to evaluate this IAS based diagnostics. Particularly, IAS signatures obtained by demodulating the frequency modulated pulse trains produced by two in-house made encoder wheels mounted at both the input and output of the PG. In addition, order spectrum analysis is applied to IAS signals to highlight fault components. IAS order spectra exhibit clear changes in the spectral amplitudes associating with different fault frequencies, showing consistent and efficient diagnostics. Besides, both the measurement system and signal processing computation for IAS based monitoring are more cost-effective and easier to be implemented online, compared with conventional vibration based methods.**

Keywords- planetary gear, torsional model, instantaneous angular speed, condition monitoring

I. INTRODUCTION

Planetary gears are widely used in aerospace, wind turbine, mine machinery industry and transportation. PG has significant advantages including high power-weight ratio and self-centering effect, which allows larger manufacturing and installation errors. Its faults usually lead to casualty and financial loss. Therefore, PG condition monitoring and diagnosis are critical to ensure safe operations and avoid significant losses due to unexpected system failures.

Most of the current PG diagnosis studies focus on understanding load sharing, processing acoustics and vibration signals, which are usually contained by strong noise and distorted system resonances. Furthermore, the symmetrical N planet structure and periodically changing transmission path make fault diagnosis process based on vibration and acoustics very challenging. Instantaneous Angular Speed (IAS), which is one of the key parameters of machine dynamics, has been shown to have vital information for diagnosis and condition monitoring [1-3]. Compared to conventional vibration and acoustics signals, IAS is less affected by transmission path and non-cyclic stationary load, which can be suppressed by rotation domain average [1].

Recently, many fault diagnosis methods based on IAS have been studied for different rotating machines. Stander [1] built a simplified gear dynamic model with four degrees of freedom and found that tooth fault with meshing stiffness reduction result in IAS changes. Yang [2] and Li [3] etc. developed a dynamic model of diesel engines, and used IAS derived from the encoder to diagnose the faults related to combustion and gas pressure. Besides, a new fault diagnosis algorithm proposed by Shao for low-speed helical gear by order tracking, angular domain synchronous average and RMS calculated in small angular ranges, which resampled in the angular domain [4]. Additionally, Leclère [5] extracted the wind turbine IAS determined from probability density function of acceleration spectrum. These studies show that the IAS allows a high-performance diagnostics to be achieved in different machines but it has not been evaluated upon a PG system.

Therefore, in this paper, a pure torsional dynamic model for one stage PG is developed firstly to identify IAS signatures due to faults on different gears and develop corresponding IAS measurement systems. Secondly, the frequency domain method for IAS calculation is examined to confirm its superiority of accuracy and anti-noise. Subsequently, a test system is set to investigate the IAS spectrums from health and different fault cases of PG for diagnosis. Finally, key conclusions are presented in implementing this IAS based PG fault diagnosis.

II. PG MODELLING AND FAULT SIMULATION

To gain an in-depth understanding of the rotation speed fluctuation caused by faulty gear in a PG, a lumped dynamic model is developed with the inclusion of sun gear fault and planet gear fault. The dynamics of PG is simplified to have pure torsional motions with $3+N$ (N is the number of planets) degree of freedom (DOF), which is efficient to have quick solutions for studying the quantitative changes in IAS signatures under different operation conditions when faults occur in different gears.

In the meantime, IAS measurement system can be configured adequately to obtain IAS signatures with sufficient accuracy for implementing the diagnostics.

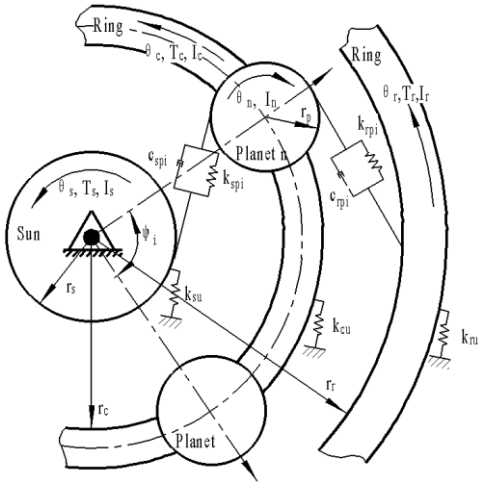

Figure 1. Rotational dynamic model of PG

A. *Planetary gear modeling*

The simplified model illustrated in Fig. 1 is composed of a sun gear (s), a carrier (c), a ring gear (r) and few planet gears ($1\cdots N$) as lumped masses. With assumptions of all components only move in the torsional direction, rigid each gear mounts, damping [6] and time-varying mesh stiffness, the equations of motion are given as [7-9]:

$$\begin{aligned}
&\frac{I_s}{r_s^2}\ddot{u}_s+\sum_{i=1}^{N}c_{sn}\dot{\delta}_{sn}+\sum_{i=1}^{N}k_{sn}\delta_{sn}+k_{su}u_s=\frac{T_s}{r_s}\\
&\frac{I_r}{r_r^2}\ddot{u}_r+\sum_{i=1}^{N}c_{rn}\dot{\delta}_{rn}+\sum_{i=1}^{N}k_{rn}\delta_{rn}+k_{ru}u_r=\frac{T_r}{r_r}\\
&\frac{I_c}{r_c^2}\ddot{u}_c-\sum_{i=1}^{N}c_{sn}\dot{\delta}_{sn}-\sum_{i=1}^{N}k_{sn}\delta_{sn}-\\
&\sum_{i=1}^{N}c_{rn}\dot{\delta}_{rn}-\sum_{i=1}^{N}k_{rn}\delta_{rn}+\sum_{i=1}^{N}k_{pn}\delta_{nt}+k_{cu}u_c=\frac{T_c}{r_c}\\
&\frac{I_p}{r_p^2}\ddot{u}_n+c_{sn}\dot{\delta}_{sn}+k_{sn}\delta_{sn}-c_{rn}\dot{\delta}_{rn}-k_{rn}\delta_{rn}c=0
\end{aligned}\tag{1}$$

where $u_x=r_x\theta_x,(x=c,r,s,1\cdots N)$ are rotational displacements, $I_x,(x=c,r,s,1\cdots N)$ are moments of inertia; k_{hn} and c_{hn} are time-varying mesh stiffness and stiffness dependent damping separately, $h=s$ (sun gear), $h=r$ (ring gear), and $n=1\cdots N$ (planetary gea4rs); T_s,T_c,T_r are external applied torque, δ_{nt} are the planet bearing tangent deformation, δ_{hn} are deformations along line of action (LOA) given as:

$$\begin{aligned}
\delta_{sn}&=u_s+u_s+e_{sn}\\
\delta_{rn}&=u_r+u_r+e_{rn}\\
\delta_{nt}&=u_c
\end{aligned}\tag{2}$$

where e_{sn} and e_{rn} are tooth geometry errors.

B. *Dynamic response charactersictics by simulation*

To gain the quantitative understanding of the PG IAS changes caused by faults, a one stage PG with 3 planets is based on to numerically investigate the rotational speed fluctuation with sun gear fault and planet gear faults. The carrier and sun gear are input and output of PG individually. The time-varying mesh stiffness is simulated as a square waveform shown in [10]. Damping, which dependents on mesh stiffness and mass, is calculated as given in [6]. The applied speed and torque on the input shaft are 140rpm and 360Nm, which correspond respectively to the 40% speed of the driving AC motor and 90% load in the test system to be depicted in coming sections. Also, the ring gear is fixed ($\theta_r=0$).The specification of the PG model listed in Table I.

TABLE I. SPECIFICATIONS OF PLANETARY GEAR

Parameters	**Components**			
	Sun	***Planet***	***Ring***	***Carrier***
Teeth number	10	26	62	
Module(mm)	2.25	2.25	2.25	
Mass(Kg)	0.29	3×0.34	3.64	2
Moments of inertia (Kg.m2×10-4)	2.1	2.9	5.05	49.3
I/r2(Kg)	0.14	0.17		1
Base circle radius (mm)	10.57	27.5	65.54	65
Pressure angle	20°	20°	20°	

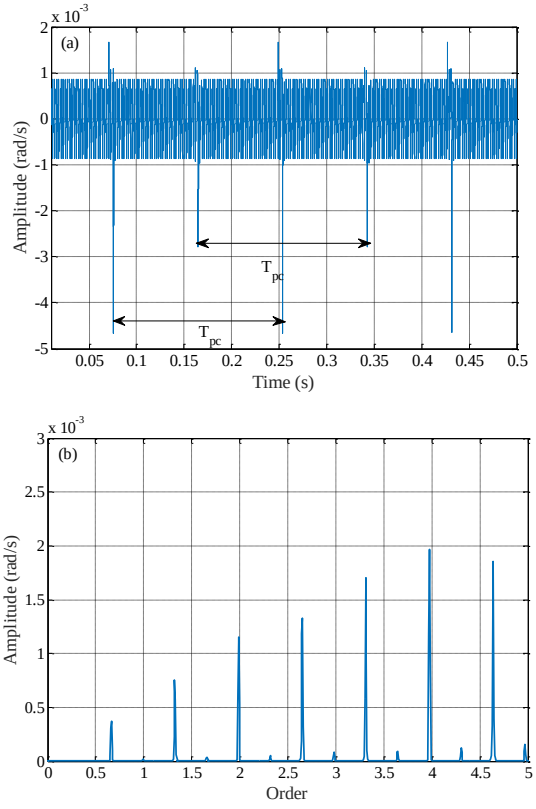

Figure 2. Rotating speed fluctuation of sun gear with planet gear fault (a) time domain (b) order spectrum

In Fig. 2 and Fig.3, the dynamic responses of sun gear rotating speed fluctuation with faults are presented both in the time domain and the shaft rotation order domain, which allows the IAS changes caused by the faults to be examined more accurately. The rotating periods of sun gear relative

Identify applicable sponsor/s here. *(sponsors)*

to carrier and planet gear relative to carrier are T_{sc}, and T_{pc}, illustrated in Fig.2 (a) and Fig. 3 (a), individually.

Fig.2 (a) and Fig. 3 (a) show clear in which impulse responses due to the periodical impacts generated by local tooth breakages. In Fig. 2 (a), it is noticeable that there are two impulses with different amplitudes in one planet rotation period T_{pc}. The IAS impulse with bigger amplitude is caused by the sun-planet fault tooth mesh. The IAS impulse with smaller amplitude is caused by the ring-planet fault tooth mesh. In Fig. 3 (a), in one sun rotation period T_{sc} impulses are related to different planets.

Spectrum lines related to faults frequencies, which is normalized by the sun gear shaft frequency, can be clearly found in Fig. 2 (b) and Fig. 3 (b). It indicates the feasibility and effectiveness of IAS based PG fault diagnosis method.

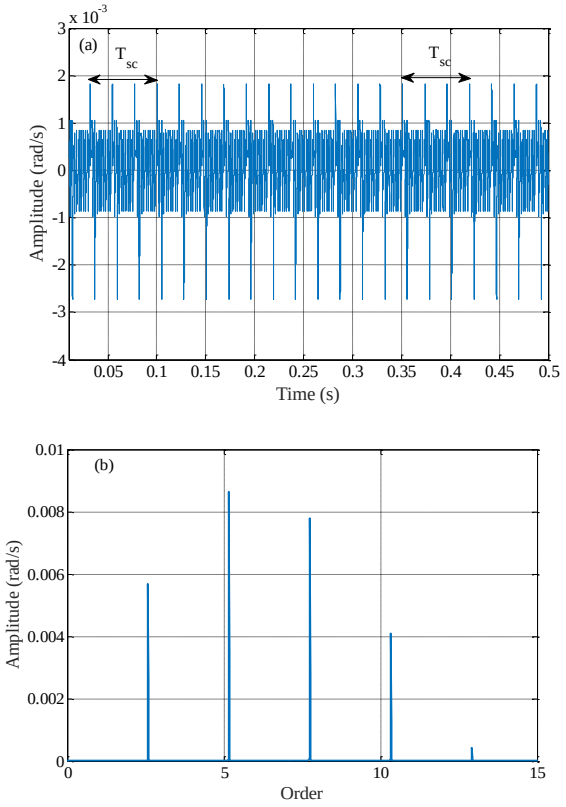

Figure 3. Rotating speed fluctuation of sun gear with sun gear fault (a) time domain (b) order spectrum

The simulation results for the faults on the sun gear and the planet gear show typical periodical oscillations of IAS. Moreover, the characteristics of theses oscillations will remain the same on the encoder wheels and do not distorted by any transmission paths, like those of conventional vibration measurements. Therefore, it paves the way for measurement configuration and signal analysis which will be addressed in forthcoming sections.

III. INSTANTANEOUS ANGULAR SPEED CALCULATION

As presented early, the periodical changes of IAS in simulation results show a clear difference between different PG faults. These IAS changes caused by PG faults lay the foundation for following signal analysis and fault diagnosis.

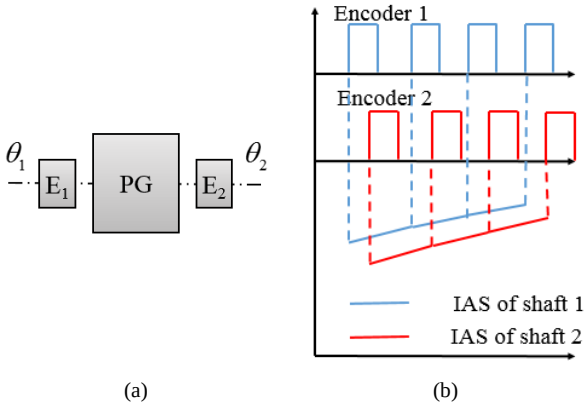

Figure 4. IAS calculation (a) schematic of encoder installation (b) pulse train and IAS

As shown in Fig. 4 (a), two encoders with optical switches are placed on carrier shaft (input) and sun gear shaft (output) of PG based on the conclusion in the previous section. In Fig. 4 (b), the IAS is calculated by the pulse train outputs of the two switches.

A. *Frequency domain method*

For more accurate and reliable IAS extraction, a frequency domain method is adapted. It uses fast Fourier transform for obtaining an analytic signal from the pulse trains, which is also more efficient for computation, compared with the direct pulse counting method. An Analytic Signal (AS) is defined as:

$$w(t) = s(t) + iH[s(t)] = A(t)e^{i\phi_s(t)} \tag{3}$$

where $s(t)$ is the raw pulse train signal, H is Hilbert transform (HT), $A(t)$ is the instantaneous amplitude, $\phi_s(t)$ is the instantaneous phase. The IAS is then calculated by:

$$\omega(t) = \frac{d\phi_s(t)}{dt} = \mathrm{Im}[\frac{\dot{w}(t)}{w(t)}] \tag{4}$$

Specifically, IAS calculation consists of following steps given in [11]:

Step 1:	FFT	$FT(f) \leftarrow F[S(t)] = \int_{-\infty}^{\infty} S(t)e^{-2\pi ift}dt$
Step 2:	HT	$AS(f) = \begin{cases} FT(f) & f \in [f_{low}, f_{high}]; \\ 0 & f \in (-\infty, f_{low}), f \in (f_{high}, +\infty); \end{cases}$
Step 3:	AS	$w(t) = F^{-1}[AS(f)] = \int_{-\infty}^{\infty} AS(f)e^{2\pi ift}df$
Step 4:	AS different iation	$\dot{w}(t) = F^{-1}[j2\pi fAS(f)] = \int_{-\infty}^{\infty} j2\pi fAS(f)e^{2\pi ift}df$
Step 5:	IAS	$\omega(t) = \mathrm{Im}[\frac{\dot{w}(t)}{w(t)}]$

B. *Encoder signal simulation*

According to the specification of the PG listed in Table I and its operating conditions, encoders mounted on the

carrier shaft and sun gear shaft need to be designed adequately so that it can reflect the characteristic events for the purpose of diagnosis. To obtain a more accurate IAS for concerned events occurring in the PG at a frequency of f_e, the encoder resolution should be higher than 20 f_e [11]. The event characteristic frequencies calculated as in [12, 13] are listed in Table II.

TABLE II. ENCODER RESOLUTION REQUIREMENT

Events	Carrier		Sun gear	
	Frequency	*Resolution*	*Frequency*	*Resolution*
Carrier rotation f_{rc}	f_{rc}	20	0.14 f_{rs}	3
Sun gear rotation f_{rs}	7.2f_{rc}	144	f_{rs}	20
Planet gear rotation f_{rp}	1.4f_{rc}	55	0.19 f_{rs}	4
Sun gear fault f_{sf}	18.6f_{rc}	369	2.58 f_{rs}	52
Planet gear fault f_{pf}	4.8f_{rc}	95	0.66 f_{rs}	14
Ring gear fault f_{rf}	3f_{rc}	60	0.42 f_{rs}	9
Gear mesh f_m	62f_{rc}	1239	8.6 f_{rs}	172

Limited by hardware performance and installation space, two 60-slot ($n_e = 60$) encoder wheels were made in house based on the test PG system based on the analysis in Table II.

To further evaluate the accuracy and reliability of IAS algorithm, an FM pulse train is simulated as:

- FM sinusoidal signal:

$$c(t) = \sin(n_e \varpi_c t + \varpi_r(t) + n(t)) \quad (5)$$

where ϖ_c is the constant rotating speed of shaft; $n(t)$ is the noise caused by disc installation errors or manufactory errors; $\varpi_r(t)$ is rotation speed fluctuation caused by fault as well as input speed variation.

- Rotation speed fluctuation simulation:

$$\varpi_r(t) = a_1 \cos(w_c t + \phi_a) + b_1 \cos(w_e t + \phi_b) \quad (6)$$

- FM pulse train transform:

$$s(t) = \begin{cases} 5000, & c(t) \geq 0 \\ 0, & c(t) < 0 \end{cases} \quad (7)$$

In Fig. 5, the theoretical IAS is simulated without any noise, the red dashed line is IAS with Gaussian white noise estimated by the FD method, which has a satisfactory accuracy in reflecting the main fluctuating profiles of IAS.

The maximum IAS measure errors given as [14]:

$$\varepsilon = \pm \frac{n_e M}{60 f_s} \quad (5)$$

where n_e is the number of encoder pulse per revolution, M is the maximum rotating speed, f_s (=96,000Hz) is the sampling frequency. At 40% AC speed condition (590rpm), encoders mounted on carrier and sun shaft have maximum IAS measure errors of 0.17% and 1.2% respectively.

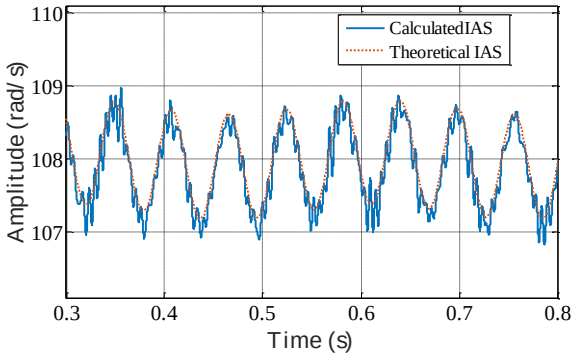

Figure 5. Simulated results under, $f_s = 96000Hz$, $a_1 = 0.4$, $b_1 = 0.3$, $w_c = 108$, $w_e = 20.5$, $\phi_a = \phi_b = 0$ and Gaussian white noise with maximum amplitude 0.02 rad

IV. EXPERIMENTAL SET-UP AND RESULT

A. Experimental set-up

The test rig, illustrated in Fig. 6 (a), is designed for evaluating the performance of PG fault diagnosis based on IAS. The whole test rig is driven by a four poles there phase 11kW Brook Crompton AC motor, which is coupled with a two stage helical gearbox for speed reduction. An 85kw DC generator applied a load to the whole test rig. The testing PG gearbox operating as a speed increaser is installed between the helical gearbox and the DC generator with two Fenner Fenaflex Tyre Couplings, so that possible torsional oscillation source from the loading DC generator, helical gearbox and AC motor can be reduced largely.

Two encoder wheels with 60 slots, illustrated in Fig.6 (b) are mounted at the low-speed input and the high-speed output, which are connected to the carrier plate and sun gear shaft respectively, in order to obtain IAS at both shafts to diagnose different faults on the sun and planet.

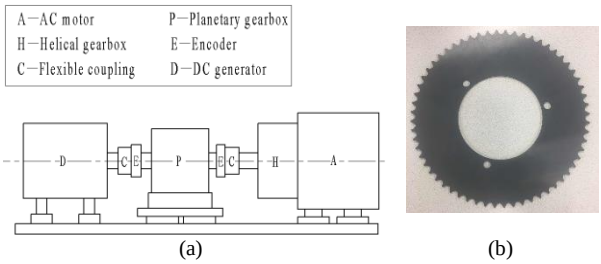

(a) (b)

Figure 6. Schematic of test rig (a) test rig (b) encoder wheel

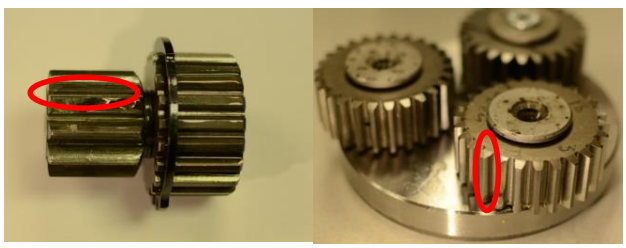

(a) (b)

Figure 7. Illustrative images of PG faults (a) sun gear tooth damage (b) planet gear tooth damage

Planet gear fault (PF) and sun gear fault (SF) illustrated in Fig. 7 (a) and (b) respectively were tested for evaluating IAS based fault diagnosis method. The teeth damages were created by removing material from the meshing face on one tooth to represent the most common failures of gear transmissions.

To evaluate the performance of IAS based PG diagnosis system, three different groups of IAS data including healthy case and two fault causes were acquired with different gear operating conditions. The healthy PG data without any faults are denoted as the baseline (BL) for further fault diagnosis. Two other groups of data were acquired with sun gear fault (SF) and planet gear fault (PF) respectively. Each group of data were collected from the PG test rig operating at 40% of AC motor full speed (1146rpm) and under 0%, 25% 50%, 75% and 90% of the 400 Nm full load.

B. Results and discussion

Fig. 8 shows IAS order spectra of the carrier at 40% speed with different loads and faults, which is calculated from the pulse train produced by the encoder wheel at the carrier, i.e. the input of PG. In addition, the frequency axis is normalized by the carrier shaft frequency, which aimed to eliminate the influences of the acreage speed errors due to operation control and aligns spectral lines for accurate comparison between tests. The IAS order spectrum lines at carrier rotating order and its harmonics are dominant. This is mainly caused by encoder wheel errors such as manufacturing and installation errors. However, these integrate orders are less correlated with the faults and have little influences on fault diagnosing.

As shown in Fig. 8 (a), planet gear fault spectra, the amplitudes at orders of 2.4, 7.2 and 12, corresponding to $0.5f_{pf}$, $1.5f_{pf}$ and$2.5f_{pf}$, are clearly higher than the baseline. The $0.5\ f_{pf}$ is the characteristic frequency of either the planet-sun fault tooth mesh or planet-ring fault tooth mesh, which are significantly reflected in IAS. Therefore, these can indicate the fault existence on the planet. However, the amplitudes at the integer orders: 7, 9, 11, 13 and 15 are also higher than baseline, which can be caused mainly by the errors of the encoder wheel. So they are not used for the diagnostics.

As shown in Fig. 8 (b), the sun gear fault spectra, the amplitudes at the order of 37.2 corresponding to $2f_{sf}$ is clearly higher than the baseline. It indicates the existing fault located in sun gear. Also, the integer orders caused mainly by encoder wheel errors as mentioned before are not used for the diagnostic.

Fig. 9 shows IAS order spectra of the sun gear at 40% speed with different loads and faults, which is calculated from the pulse train produced by the encoder wheel connected with the sun gear, i.e. the output of PG. The frequency axis is also normalized by the sun gear shaft frequency. The IAS order spectrum lines at sun gear rotating orders and its harmonics are more dominant. As mentioned before, this is mainly caused by the errors of the encoder wheel during manufacturing and installation.

As shown in Fig. 9 (a), the planet gear fault spectra, the amplitudes at orders of 0.33, 2, and 3, corresponding to $0.5f_{pf}$, $3f_{pf}$, and $4.5f_{pf}$, are clearly higher than the baseline. These changes can effectively indicate the presence of the fault located in planet gear.

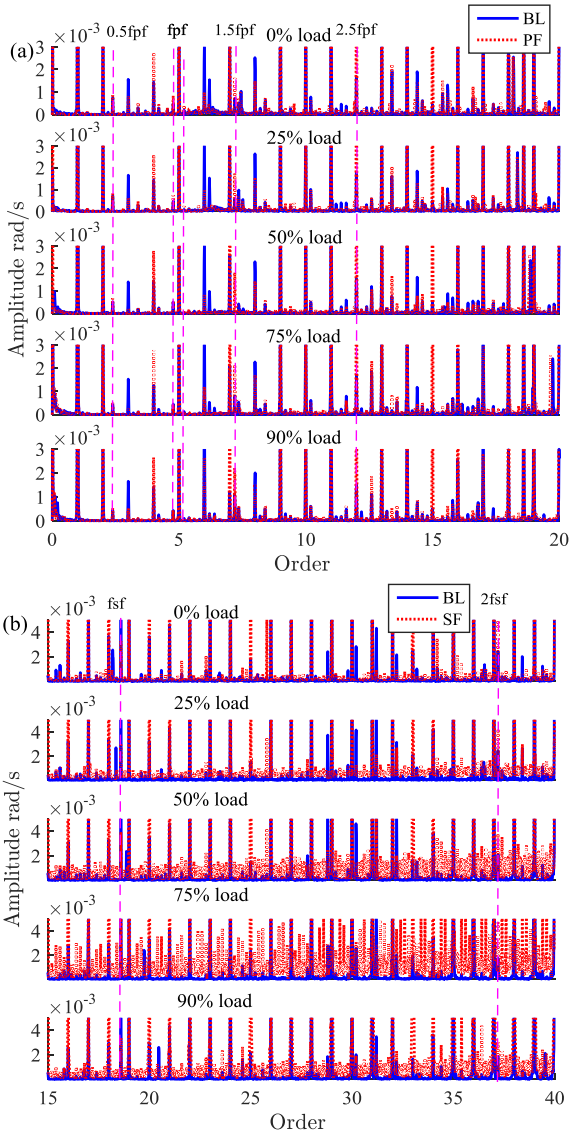

Figure 8. IAS order spectrum of carrier under 40% speed (a) planet gear fault (b) sun gear fault

As shown in Fig. 9 (b), the sun gear fault spectra, the amplitudes at orders of 5.17, 6.75, 7.75, 8.75, 9.75 and 10.3 correspond to $2f_{sf}$, $3f_{sf}-f_{sr}$, $3f_{sf}$, $3f_{sf}+f_{sr}$, $3f_{sf}+2f_{sr}$ and $4f_{sf}$ are higher than baseline, which shows the evidence of existing fault located in sun gear. The integer orders mainly contributed by encoder wheel errors are not considered as an indicator in fault diagnosis.

Based on above analysis and the findings from dynamic simulation aforementioned, the method proposed in this paper can be effectively used to diagnose PG faults.

V. CONCLUSION

This study has shown that the proposed IAS based PG diagnosis system can be effective to monitoring faults from

the gearbox system under a wide range of operating conditions. Especially, the fault signature associating with planet gear can be identified based on the increase in the fault related fractional orders. By contrast, these fault-related signatures are usually very difficult for conventional vibration based methods to be detected. In addition, the fault diagnosis can be realized by using either of the encoders installed on the input and the output of the PG.

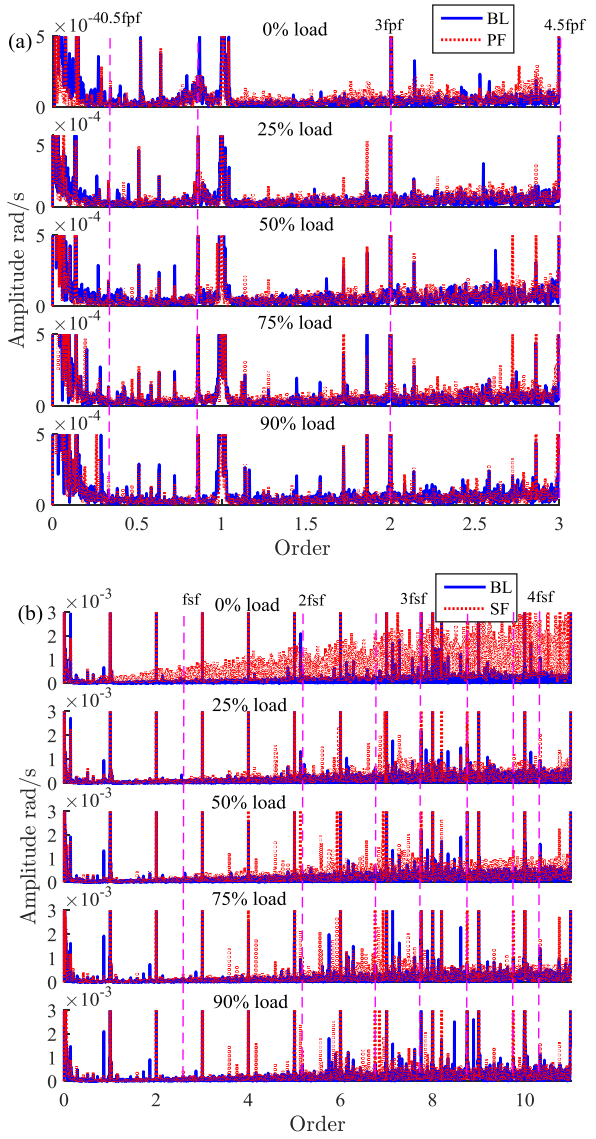

Figure 9. IAS order spectrum of sun gear under 40% speed (a) planet gear fault (b) sun gear fault

Based on the torsional dynamic model and simulation analysis, the IAS diagnostic signatures are characterised for IAS signal processing and for IAS measurement system configuration. In general, this IAS based diagnostic system can be deployed for online monitoring at low hardware cost, medium signal processing.

Further study will investigate more effective ways to improve the measurement accuracy by reducing the influences of encoder wheel errors.

ACKNOWLEDGMENT

The authors are grateful for the financial support provided by the National Natural Science Foundation of China under Contract No. 51475053 and China Scholarship Council No. 201606050039.

REFERENCES

[1] Stander, C. and P. Heyns, "Instantaneous angular speed monitoring of gearboxes under non-cyclic stationary load conditions," Mechanical Systems and Signal Processing, 2005. 19(4): p. 817-835.

[2] Yang, J., Pu, L., Wang, Z., Zhou, Y. and Yan, X., "Fault detection in a diesel engine by analysing the instantaneous angular speed," Mechanical systems and signal processing, 2001. 15(3): p. 549-564.

[3] Li, Z., Yan, X., Yuan, C. and Peng, Z., "Intelligent fault diagnosis method for marine diesel engines using instantaneous angular speed, " Journal of Mechanical Science and Technology, 2012. 26(8): p. 2413-2423.

[4] Shao, Y., Su, D.,Al-Habaibeh, A.and Yu, W., "A new fault diagnosis algorithm for helical gears rotating at low speed using an optical encoder," Measurement, 2016. 93: p. 449-459.

[5] Leclère, Q., H. André, and J. Antoni, "A multi-order probabilistic approach for Instantaneous Angular Speed tracking debriefing of the CMMNO′ 14 diagnosis contest," Mechanical Systems and Signal Processing, 2016. 81: p. 375-386.

[6] August, R., "Dynamics of planetary gear trains," Vol. 3793. 1984: National Aeronautics and Space Administration, Scientific and Technical Information Branch.

[7] Geramitcioski, T. and L. Trajcevski., "Theoretical improvement of the planetary gear dynamic model," in DS 30: Proceedings of DESIGN 2002, the 7th International Design Conference, Dubrovnik. 2002.

[8] Al-Shyyab, A. and A. Kahraman, "A non-linear dynamic model for planetary gear sets," Proceedings of the Institution of Mechanical Engineers, Part K: Journal of Multi-body Dynamics, 2007. 221(4): p. 567-576.

[9] Cheng, Z., Hu, N., Gu, F. and Qin, G., "Pitting damage levels estimation for planetary gear sets based on model simulation and grey relational analysis," Transactions of the Canadian Society for Mechanical Engineering, 2011. 35(3): p. 403-417.

[10] Chaari, F., T. Fakhfakh, and M. Haddar, "Dynamic analysis of a planetary gear failure caused by tooth pitting and cracking," Journal of Failure Analysis and Prevention, 2006. 6(2): p. 73-78.

[11] Gu, F., Yesilyurt, I.,Li, Y., Harris, G, and Ball, A., "An investigation of the effects of measurement noise in the use of instantaneous angular speed for machine diagnosis," Mechanical Systems and Signal Processing, 2006. 20(6): p. 1444-1460.

[12] Tian, X., Abdallaa, G., Rehab, I., Gu, F., Ball, A. and Wang, T., "Diagnosis of combination faults in a planetary gearbox using a modulation signal bispectrum based sideband estimator," in Automation and Computing (ICAC), 2015 21st International Conference on. 2015. IEEE.

[13] Feng, Z. and M.J. Zuo, "Vibration signal models for fault diagnosis of planetary gearboxes," Journal of Sound and Vibration, 2012. 331(22): p. 4919-4939.

[14] Li, Y., Gu, F., Harris, G., Ball, A., Bennett, N. and Travis, K., "The measurement of instantaneous angular speed," Mechanical Systems and Signal Processing, 2005. 19(4): p. 786-805.